J. Fluid Mech. (1975), *vol.* 71, *part* 2, *pp.* 317–338
Printed in Great Britain

Turbulence measurements in an 'equilibrium' axisymmetric wall jet

By B. R. RAMAPRIAN

Department of Aeronautical Engineering, Indian Institute of Science, Bangalore

(Received 10 September 1974)

This paper reports measurements of turbulent quantities in an axisymmetric wall jet subjected to an adverse pressure gradient in a conical diffuser, in such a way that a suitably defined pressure-gradient parameter is everywhere small. Self-similarity is observed in the mean velocity profile, as well as the profiles of many turbulent quantities at sufficiently large distances from the injection slot. Autocorrelation measurements indicate that, in the region of turbulent production, the time scale of v fluctuations is very much smaller than the time scale of u fluctuations. Based on the data on these time scales, a possible model is proposed for the Reynolds stress. One-dimensional energy spectra are obtained for the u, v and w components at several points in the wall jet. It is found that self-similarity is exhibited by the one-dimensional wavenumber spectrum of $\overline{q^2}$ ($= \overline{u^2}+\overline{v^2}+\overline{w^2}$), if the half-width of the wall jet and the local mean velocity are used for forming the non-dimensional wavenumber. Both the autocorrelation curves and the spectra indicate the existence of periodicity in the flow. The rate of dissipation of turbulent energy is estimated from the $\overline{q^2}$ spectra, using a slightly modified version of a previously suggested method.

1. Introduction

Turbulent wall jets find application in many practical situations, such as film cooling, boundary-layer control, etc. There are several investigations reported on wall jets. Most of these investigations pertain to the study of the mean flow quantities in the wall jet. Only in a few cases have data on the turbulence quantities been reported. Kruka & Eskinazi (1964) reported data on turbulent intensities and the turbulent shear stress in a plane wall jet subjected to zero pressure gradient. Kacker & Whitelaw (1968) also studied zero-pressure-gradient plane wall jets. They obtained, in addition to turbulent intensities and turbulent shear, the integral length-scale distribution across the wall jet, by making cross-correlation measurements. Newman *et al.* (1972) reported measurements of u' along the centre-line of a three-dimensional wall jet originating from a circular orifice. The author is not aware of any report on turbulence measurements in plane or axisymmetric wall jets subjected to adverse pressure gradients. Ramaprian (1973) reported a study of the mean flow properties of axisymmetric wall jets in conical diffusers. The wall jet in this study was obtained by injecting into the main flow a stream of high velocity fluid tangentially along the wall of

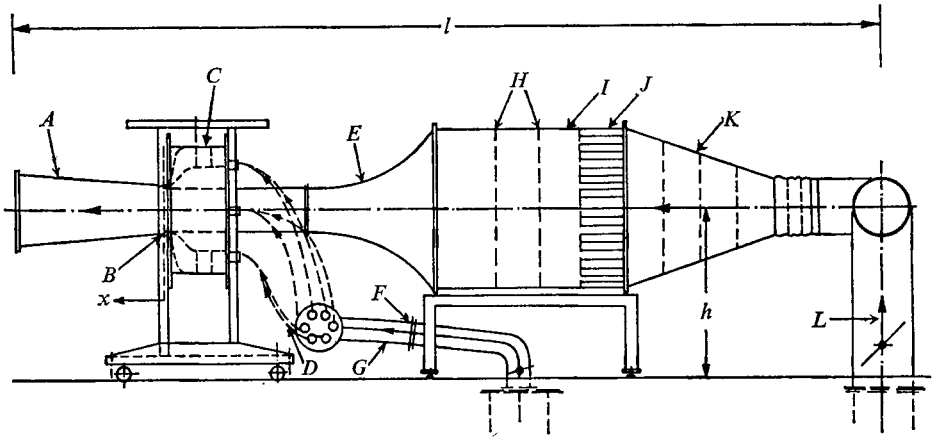

FIGURE 1. Layout of the apparatus. $l = 20$ ft approx., $h = 4$ ft. A, test diffuser; B, injection slot; C, annualar settling chamber; D, hose pipes; E, contraction nozzle; F, orifice meter; G, secondary air; H, sixteen-mesh screens; I, settling chamber; J, honeycomb; K, decelerating duct; L, main air.

the diffuser, through an annular slot situated at the inlet. Different wall-jet configurations were obtained by using different injection velocities and diffusers of different half-angles. It was found that, in general, wall-jet development was too complicated to be described by universal algebraic expressions, and required the solution of the governing differential equation in each case. But it was found that, under one condition, the wall-jet behaviour exhibited a relatively simple universal trend. This condition was that a non-dimensional pressure-gradient parameter

$$\beta = \frac{y_m}{\tau_w}\frac{dp}{dx}$$

should be 'small' (say $\lesssim 4$). (y_m is the distance of the point of maximum velocity from the wall; τ_w is the wall shear stress; and dp/dx is the longitudinal pressure gradient.) Under this condition, the behaviour of the wall jet could be correlated with that of the zero-pressure-gradient, plane wall jet of Kruka & Eskinazi, using suitably stretched parameters to account merely for the geometry of the diffuser. This observation provided the inspiration for the present study. While the value of β in this special case is small, it does not necessarily mean that dp/dx is small. In fact, such wall jets can be associated with fairly large pressure gradients.

2. The present investigation

The present paper reports a detailed study of an axisymmetric wall jet subjected to an adverse pressure gradient, in such a manner that β is everywhere roughly 2. The pressure gradient dp/dx is *not* arbitrary, but decided by the interaction of the boundary layer and 'core' flow inside the diffuser. This interaction itself was discussed by Nicoll & Ramaprian (1970); and it will not be discussed again here. It is relevant to mention that it appears that, at small values of β, the pressure gradient gets so set-up as to result in a wall jet which behaves,

in some sense, like a zero-pressure-gradient plane wall jet. It will be shown in this paper that such a wall jet exhibs approximate self-similaritity, in both mean and turbulent properties, at sufficiently large distances from the slot. Such a wall jet will be referred to as an 'equilibrium' wall jet. It provides an opportunity to study the equilibrium structure of turbulence in highly sheared wall flows. It is expected that the results obtained here for axisymmetric flow will be generally applicable to plane flows, as well.

2.1. *Experimental apparatus*

The present study was confined to a wall jet developed in a diffuser of half-cone angle 5°. The diffuser had an inlet diameter of 12 in. and a nominal area ratio of 3. The inlet velocity of air flowing through the diffuser was about 70 ft s^{-1} and the velocity of the injected air through the quarter-inch annular slot was about 120 ft s^{-1}. A schematic layout of the experimental apparatus is shown in figure 1. A more detailed description of the apparatus appears in Ramaprian (1969, 1973). Hot-wire traverses were made at several longitudinal stations, in a direction normal to the diffuser wall. These stations correspond to x/t_c values of 10, 22, 46, 70, 94 and 118, respectively (t_c is the width of the slot.)

2.2. *Instrumentation*

The mean velocity profiles in the wall-jet layer were measured using a total head tube of 0·028 in. outside diameter and wall static taps. The wall shear stress was measured using a Preston tube of a diameter sufficiently small that it was fully submerged in the buffer layer, where the law of the wall has been found not to be different from that in fully-developed pipe flow. (See Kruka & Eskinazi 1964.) Also, the Preston tube data agreed, to within 5 %, with the values obtained by extrapolation to the wall of the shear-stress data obtained from hot-wire measurements. The mean velocity data obtained from the total head tube were later used to calibrate the readings of the hot-wire probe at each station. The hot-wire probe was essentially used to measure turbulence quantities only. The hot-wire equipment consisted of two channels of DISA constant-temperature anemometers, each with a linearizer. A miniature X-probe was used to measure the turbulence intensities u', v' and w' and the Reynolds stress $-\rho\overline{uv}$. A DISA correlator was used to isolate the u and v (or u and w) signals by the usual method of summing and differencing the instantaneous outputs of the two channels, which were proportional to $u+v$ and $u-v$ (or $(u+w$ and $u-w)$, respectively. The wires were made as nearly identical as possible. The sensitivities of the two wires were finally equalized by adjusting the overheats of the two wires slightly. The probe was aligned in the stream by ensuring that the mean outputs of the two channels did not differ from each other by more than 1 % anywhere across the wall jet. No correction was applied for the effect of wire separation on the measured values of u, v and w. Since the wire separation was of the order of the microscale of turbulence, no significant errors are expected in the measurements of intensities, the integral time scales or energy spectra, in the wavenumber range discussed in this paper. The Reynolds stress was obtained from the difference between $\overline{(u+v)^2}$ and $\overline{(u-v)^2}$.

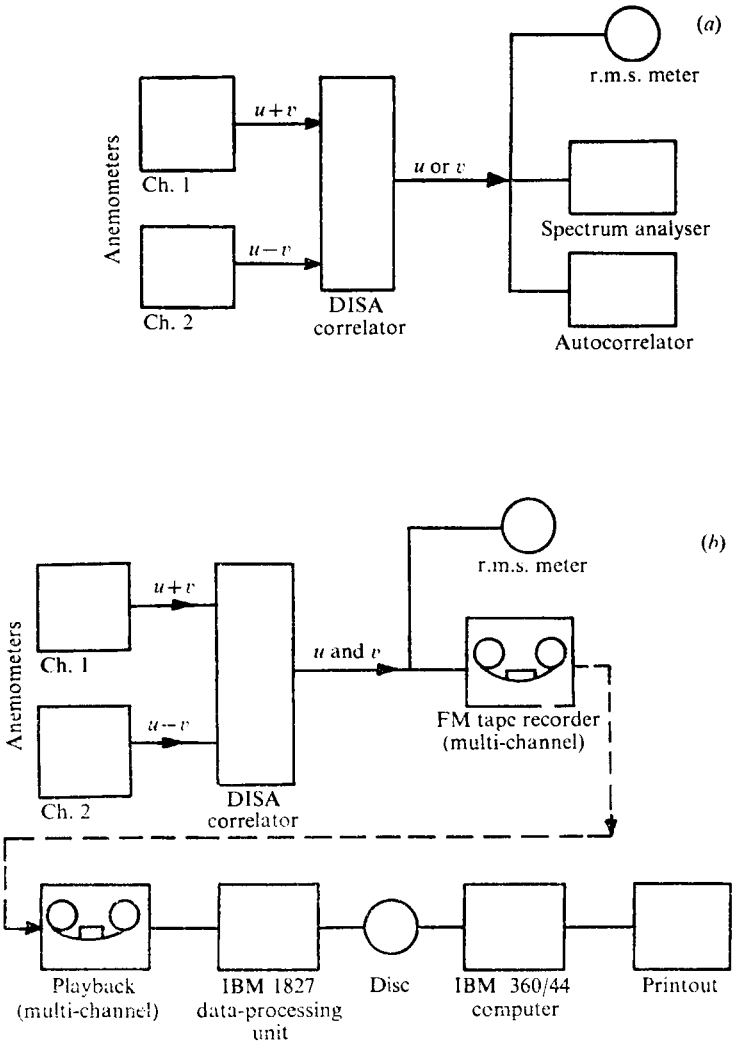

FIGURE 2. Block diagram of instrumentation.

The data were processed according to two different schemes, as shown in the block diagram in figure 2. Scheme (*a*) consisted of an r.m.s. meter for obtaining r.m.s. values, a B & K spectrum analyser (with a range of 2–20000 Hz and a bandwidth of $\frac{1}{3}$ octave) for spectrum analysis, and a Princeton Signal Correlator for autocorrelation study of the u, v and w signals. The arrangement was used only in the initial stages, to check the satisfactoriness of scheme (*b*).

Scheme (*b*) consisted of recording the u and v (or u and w, as the case may be) signals from the DISA correlator on a magnetic tape using a Hewlett–Packard FM tape recorder (bandwidth 0–10 kHz) at a tape speed of 60 in. s^{-1}. Before recording, the signals were passed through a sharp cut-off low-pass filter, set to cut off nominally at 10 kHz, to limit the bandwidth of the signal. This filter setting, which give a flat frequency response up to 6 kHz, was selected after ensuring, during preliminary studies, that it had no observable effect on the r.m.s.

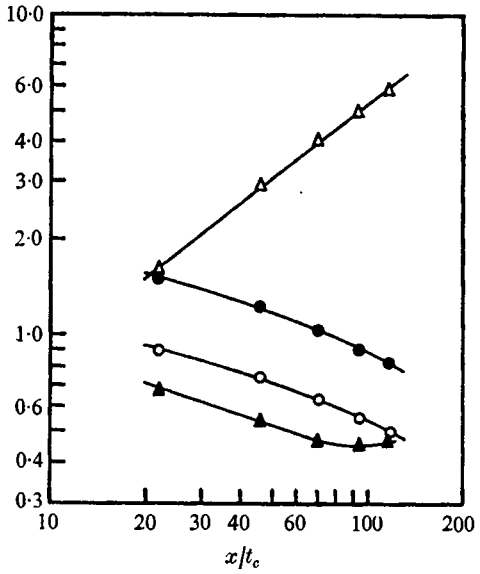

FIGURE 3. The longitudinal distribution of some of the wall-jet parameters. —○—, $\bar{U}_e/\bar{U}_0$; —●—, $\bar{U}_m/\bar{U}_0$; —△—, $y_{\frac{1}{2}}/t_c$; —▲—, $\tau_w/\rho\bar{U}_e^2$.

values of the signals. The signals were later played back at a quarter of the recording speed. The output signal was digitized, stored on disc, and later processed on an IBM 360/44 computer, using an IBM 1827 data-processing system. Usual precautions were taken to check and control any distortion or deterioration of the signal in the course of recording and play-back. The digitization of the signal was done by an analog–digital converter, driven at a sampling frequency of 10 kHz, and set to sample the u and v (or u and w) signals alternately. This amounted to a sampling frequency of 5 kHz for each component, in terms of the play-back speed, and corresponded to a real-time sampling frequency of 20 kHz of the recorded signals. With this sampling frequency, the spectrum in the range of 6–10 kHz would be aliased by the spectrum in the range of 10–14 kHz. The low-pass filter set at 10 kHz ensured that error due to this aliasing was negligible.

Digital analysis was made using 3000 samples in a batch, and subsequently averaging over 30 batches. These 30 batches were selected at uniform time intervals over 30 s of real time. This procedure was adopted to combine long-time averaging with practical feasibility, in terms of computer time and memory size. D.c. and very low frequencies were removed by digital filtering, to avoid distortions in spectral density in the neighbourhood of zero frequency, as well as to improve the stability of statistical estimates. Autocorrelation coefficients were obtained by calculating the time-averaged lagged products for various time-delays. Power spectra were obtained *directly* from the signal samples, using the technique of discrete fast Fourier transform. The accuracies of these calculations will be discussed later, in § 6. It will be mentioned here only that the data-processing scheme was designed in accordance with standard practice, so as to obtain the best possible accuracy with the available data-processing facility.

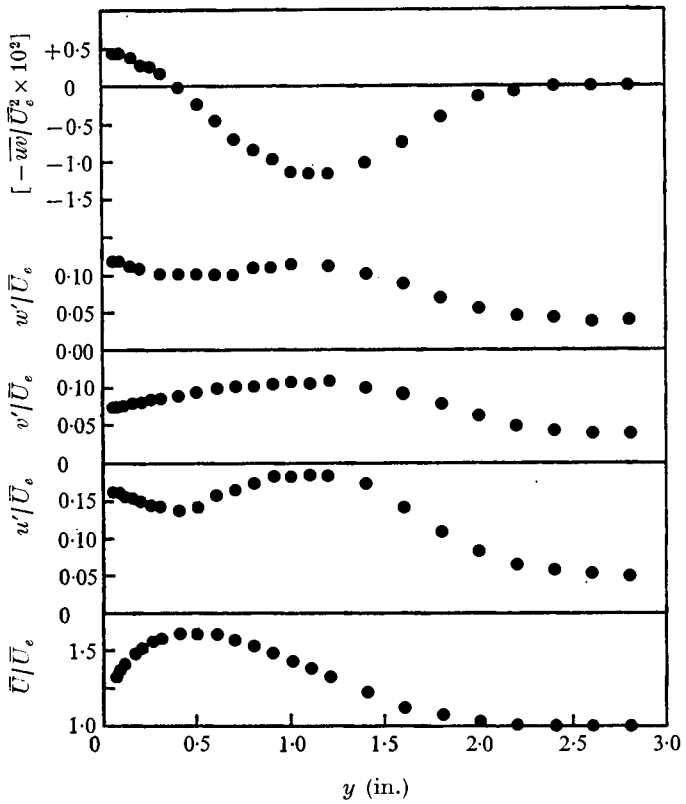

FIGURE 4. Distribution of the mean and turbulent quantities across the wall jet at $x/t_c = 94$.

(See e.g. Blackman & Tukey 1958.) The spectrum and correlation results obtained digitally were compared in a few test cases with the results obtained from the procedure mentioned in scheme (*a*), viz. from the spectrum analyser and signal correlator. They were found satisfactory.

3. Results

Figure 3 shows the longitudinal distribution of some of the important gross parameters of the wall jet, such as the free-stream (diffuser centre-line) velocity $\overline{U}_c$, the maximum velocity in the wall jet $\overline{U}_m$, the half-width of the wall jet $y_{\frac{1}{2}}$ and the local skin-friction coefficient $\frac{1}{2}C_f$. ($y_{\frac{1}{2}}$ is defined as the distance from the wall to the point where the velocity is $\frac{1}{2}[\overline{U}_m + \overline{U}_{\mathrm{min}}]$. $\overline{U}_{\mathrm{min}}$ is the minimum velocity in the section. $\frac{1}{2}C_f$ is defined as $\tau_w/\rho\overline{U}_e^2$. $\overline{U}_e$ and $\overline{U}_m$ have been normalized with respect to $\overline{U}_0$, the free-stream velocity in the plane of the slot exit.) The value of the pressure-gradient parameter β for this flow was everywhere about 2. Ramaprian (1973) showed that the wall-jet development under this condition could be correlated with that of a two-dimensional plane wall jet, using suitably stretched parameters.

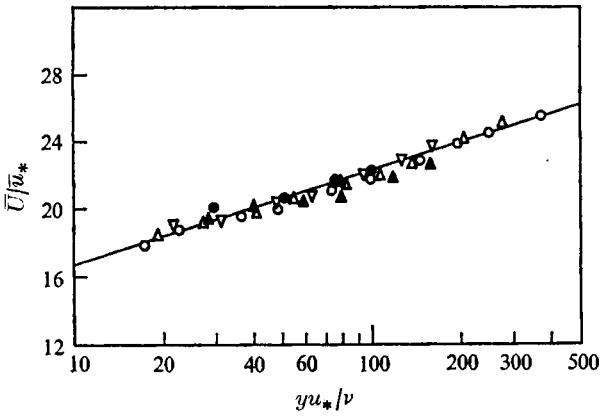

FIGURE 5. Mean velocity distribution adjacent to the wall. x/t_c: ●, 22; ▲, 46; ▽, 70; △, 94; ○, 118. ——, distribution $\bar{U}/u_* = 5{\cdot}5 \log yu_*/\nu + 11{\cdot}2$, from Ramaprian (1973).

The distributions across the wall jet of the mean velocity $\bar{U}$, the three turbulent velocity components u', v' and w', and the Reynolds shear stress $-\rho\overline{uv}$ were obtained at different longitudinal positions along the diffuser wall. However, only one set of typical profiles is shown in figure 4. From this figure, the following important observations can be made.

(i) The turbulent shear stress attains a very large negative value inside the wall jet (more than twice the positive value at the wall). Reference to the literature indicates that, while the present wall jet behaves in its gross features like the plane zero-pressure-gradient, two-dimensional wall jet of Kruka & Eskinazi or Kacker & Whitelaw, the shear stress in the present case reaches much larger negative magnitudes than in the other cases for the same ratio $\bar{U}_j/\bar{U}_0$, where $\bar{U}_j$ is the velocity through the slot. The large negative shear stress in the present case is a result of the rapid deceleration of the main stream, causing a large difference in velocity across the jet-like outer region of the wall jet. Thus, the present wall jet reproduces the situation of a strong adverse pressure gradient; but it is so generated that it results in a low value of β.

(ii) The turbulent shear stress passes through zero at a distance from the wall slightly smaller than the distance of the point where the mean velocity attains its maximum. This fact has been observed in the other experiments on wall jets, also referred to previously. It presents some difficulty in using Boussinesq-type effective viscosity models to describe wall-jet behaviour.

(iii) All the components of turbulent fluctuations reach a local maximum in the outer region of the wall jet at about the same point as that at which shear stress reaches its maximum negative value. Likewise, the turbulent energy attains a local minimum around the point where the shear stress is zero. The latter fact is more clearly observed from figures 7 and 8.

The distribution of mean velocity adjacent to the wall is shown in a semi-logarithmic plot in figure 5. A nearly universal distribution is observed that agrees, to within 5 %, with the distribution.

$$\bar{U}/u_* = 5{\cdot}5 \log yu_*/\nu + 11{\cdot}2$$

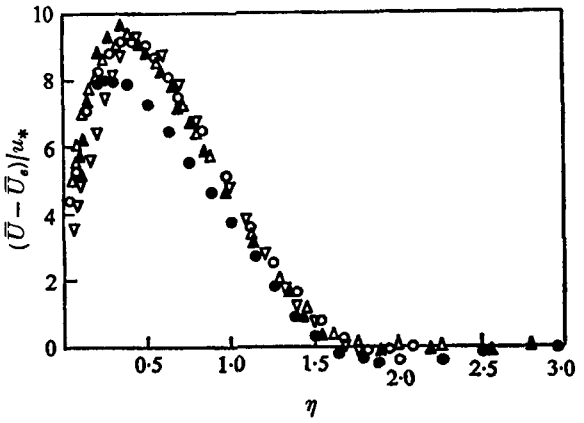

FIGURE 6. Mean velocity profiles in defect co-ordinates. Symbols as in figure 5.

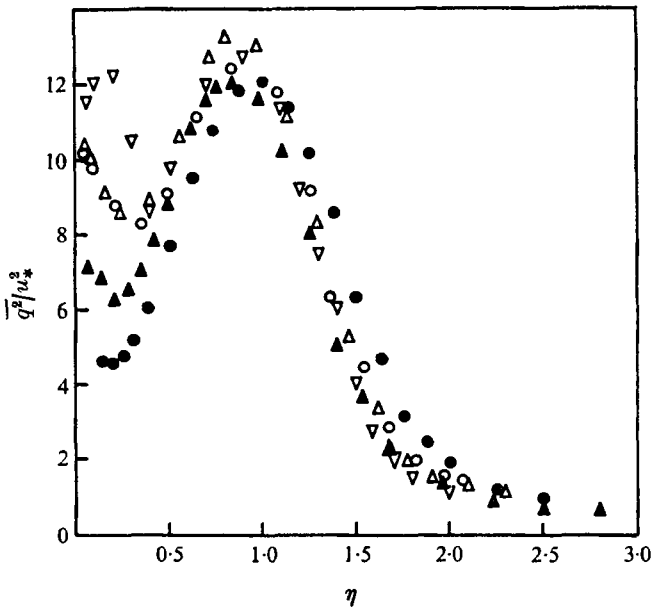

FIGURE 7. Distribution of $\overline{q^2}$ across the wall jet. Symbols as in figure 5.

of Ramaprian (1973). It is particularly important to note that the additive constant in the log law is very much higher than the value for conventional boundary layers.

Figures 6–8 present the distribution of the velocity 'defect' $(\overline{U}-\overline{U}_e)$, the turbulent quantity $\overline{q^2}$ $(= u'^2+v'^2+w'^2)$ and the Reynolds shear stress $-\rho\overline{uv}$, wherein the variables have been normalized using the outer-layer velocity and length scales u_* and $y_{\frac{1}{2}}$, respectively. From the three figures, it can be seen that the flow attains self-preservation over the outer region $(y/y_{\frac{1}{2}} = \eta > 0{\cdot}5$, say) for sufficiently large values of x/t_c. The mean velocity profile exhibits self-preservation at smaller values of x/t_c and η when compared with the $\overline{q^2}$ and $\overline{uv}$ profiles. These self-similar profiles indicate that the wall jet has attained a state of structural equilibrium,

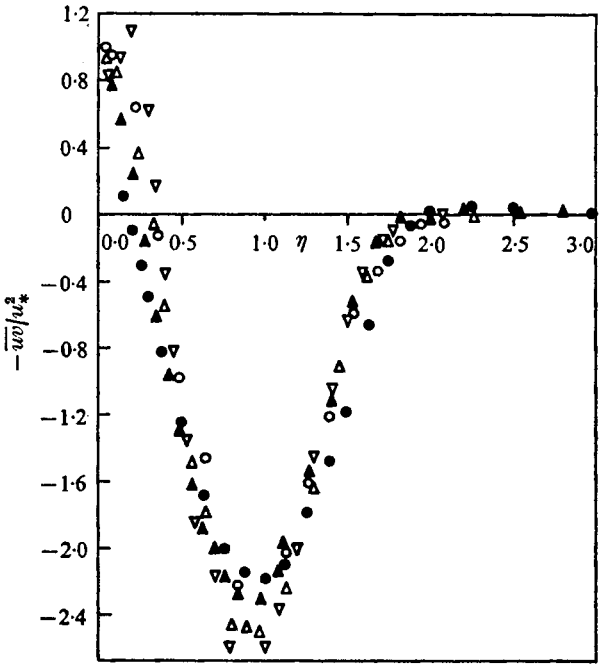

FIGURE 8. Distribution of the Reynolds shear stress across the wall jet. Symbols as in figure 5.

at least in the outer layer. This quasi-equilibrium makes it worthwhile to study the structure of this highly-sheared turbulent flow in somewhat greater detail. Something of this is reported in the rest of the paper.

4. Implications of the phenomenological hypotheses

The present data allow one to compare the implications and relative usefulness of commonly-used shear-stress hypotheses. Three such hypotheses are considered here. These are as follows. (i) The *Prandtl mixing-length hypothesis*

$$\tau = \rho l_m^2 \left|\frac{\partial \overline{U}}{\partial y}\right| \frac{\partial \overline{U}}{\partial y} \tag{4.1}$$

(τ is the shear stress; and l_m is the mixing length at any point). (ii) The *Prandtl–Kolmogorov hypothesis* (Kolmogorov 1942)

$$\tau = C_\mu \rho (\overline{q^2})^{\frac{1}{2}} l_k \frac{\partial \overline{U}}{\partial y} \tag{4.2}$$

(l_k is a length scale; and C_μ is a universal constant). (iii) The *Bradshaw hypothesis* (Bradshaw, Ferriss & Atwell 1967)

$$\tau = \rho a \overline{q^2} \tag{4.3}$$

(a is a universal constant).

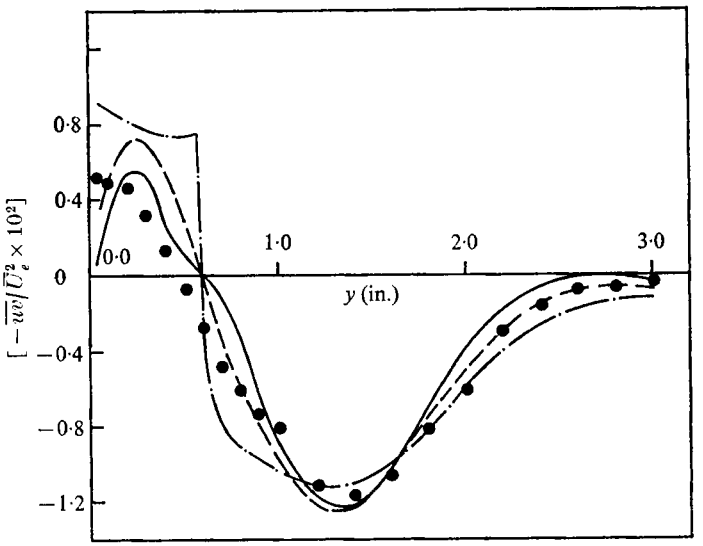

FIGURE 9. Comparison of the calculated shear-stress distribution with measurements at $x/t_c = 118$. ●, measurement; ——, calculated from Prandtl mixing-length hypothesis, with $\kappa = 0{\cdot}4$ and $\lambda = 0{\cdot}15$; – – – –, calculated from Prandtl–Kolmogorov hypothesis, with $l_k = l_m$ and $C_\mu = 0{\cdot}63$; —·—·—, calculated from Bradshaw hypothesis, with $a = 0{\cdot}175$.

The hypotheses (4.1) and (4.2) are often used in boundary-layer calculations, along with a simple two-layer hypothesis for the distribution of the length scale, of the form

$$l = \kappa y \quad \text{for} \quad 0 < y < \lambda y_{\frac{1}{2}}/\kappa, \qquad l = \lambda y_{\frac{1}{2}} \quad \text{for} \quad y \geqslant \lambda y_{\frac{1}{2}}/\kappa. \tag{4.4}$$

(κ and λ are universal constants.) The implications of these hypotheses in the case of the present wall-jet flow are seen from figure 9, where the shear-stress distributions computed from (4.1) and (4.2), using the above two-layer length scale model, are compared with measurements at station $x/t_c = 118$. The value of κ was taken as 0·4; and l_k was assumed to be equal to l_m everywhere. The values of $\lambda = 0{\cdot}15$ and $C_\mu = 0{\cdot}63$ were selected so as to give the best fit to the experimental data. It is seen that both the simple hypotheses do yield a reasonably satisfactory shear-stress distribution in the outer layer. In the wall layer, however, the hypotheses are seen to be unsatisfactory. Also, though the gradient models cannot predict the observed non-zero shear stress at the point of maximum velocity, this is not very serious, as the shear stress is very small in this region.

The shear-stress distribution calculated from (4.3) is also seen in figure 9. For this hypothesis to be applicable to the wall jet, one must attach the proper sign to τ in it. It has been assumed here that τ will have the sign of $\partial \bar{U}/\partial y$. The value of a was taken as 0·175, which gave the best fit to the experimental data. The hypothesis is also seen to fare reasonably well in the outer region, but very poorly in the inner.

5. Autocorrelation measurements

Wall-jet flow provides an opportunity of studying a highly-sheared flow with the following features. (i) The direction of the shear changes across the shear layer. (ii) There is a strong interaction between the wall and free shear flow. (iii) Considerable turbulence is generated sufficiently far from the wall that X-wire measurements can be made easily.

The turbulent energy in the region of production is seen from figure 4 to be large, non-homogeneous and anisotropic. Thus, it was felt that it would be worthwhile to study how the length or time scales of the different components u', v' and w' behaved across the wall jet. It would be particularly useful to know whether these scales also exhibit anisotropy and non-homogeneity, and, if so, whether a relevant and dominant scale can still be usefully identified. Further, such a study might lead to a little more information on the wall layer, which has been seen from figure 5 to behave differently from a conventional boundary layer.

Length-scale measurements of u fluctuations in a wall jet were obtained by Kacker & Whitelaw (1968) from measurements of space correlations. In the present work, it was decided to obtain data on autocorrelation functions of u, v and w components of turbulence. The autocorrelation measurements are not a substitute for space-correlation measurements, however. In fact, from the present measurements, only three of the nine length scales at a point can be obtained. The decision to make autocorrelation measurements was made primarily because of the relative ease with which autocorrelation data could be obtained, especially when a digital data-processing facility was available. Incidentally, time-correlation measurements have the advantage that they involve single-point measurements, while space-correlation measurements require two-point measurements. Single-point measurement enables one to obtain a local scale at a point. Further, it eliminates the errors introduced by mutual probe interference, inherent in multi-probe measurements.

The autocorrelation coefficient for (say) the u component of the turbulent velocity at a point (x, y), for a time separation T, is defined as

$$R_u(x, y, T) = \overline{u(x, y, t)\, u(x, y, t+T)}/\overline{u^2}(x, y). \tag{5.1}$$

(The overbar represents time averaging.)

Autocorrelation data for u, v and w components were obtained at several points across the wall jet, at two stations ($x/t_c = 22$ and 118). More than 80 correlation curves were obtained in all. Only one typical set is shown in figure 10. At the scanning speeds used for digitization, the autocorrelation coefficient R could be obtained at time steps ΔT of $0{\cdot}5 \times 10^{-4}$ s. If a typical inner-layer time scale T_w is defined as

$$T_w = \nu/u_*^2, \tag{5.2}$$

the time step used corresponds to a non-dimensional time interval $\Delta T/T_w$ in the range 1–6. The length of signal sampled was 80 ms in all the cases, which corresponds to a non-dimensional time in the range 1600–10 000. Thus, digital sampling and analysis provides the possibility of high resolution and long length of the correlogram simultaneously (a feature not easily achieved with analog

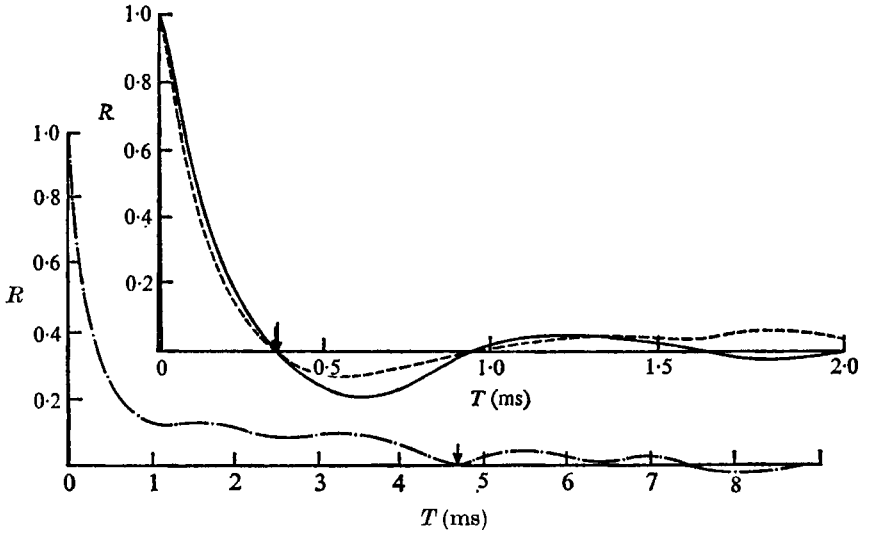

FIGURE 10. Autocorrelation curves of u', v' and w' at $x/t_c = 22$ and $y = 0{\cdot}4$ in. —·—·—, R_u; ——, R_v; – – – – –, R_w. Arrows indicate the 'last point' on the correlation curve for computing the area under the curve.

correlators). As mentioned already, each correlation curve was obtained as an average of 30 correlograms taken over a period of 30 s. For obtaining each correlation curve, averaging was done over a total number of samples varying from 30×1400–30×3000. The smaller value corresponded to a time lag of 80 ms, and the larger to that of 0·05 ms. A rough estimate of the accuracy of the correlation data can be made by calculating e, the ratio of the standard deviation to the mean value of the correlation coefficient R. e is given approximately by the expression

$$e = (1 + R^{-2})^{\frac{1}{2}}/(2BT_s)^{\frac{1}{2}}.$$

(See Magrab & Blomquist 1971. B is the bandwidth of the signal in hertz (10000 in the present case); and T_s is the total duration of the record (30 s in the present case).) e works out to be about 0·025 for $R = 0{\cdot}05$, indicating that the averaging procedure is fairly satisfactory.

The following comments can be made about the correlation curves. (i) As seen from the typical curves in figure 10, the correlation curves did not come out as smooth functions going to zero at large values of T, as is usually obtained from analog correlators. Quite a few of the curves exhibited negative loops. The loops were found to be particularly strong for v and w components. (ii) The typical curves in figure 10 also indicate the difficulty in the definition of an integral time scale. It was decided in the present study to treat the point where the curve *first* crossed the x axis as the 'last' point on the correlation curve. The area under the curve up to this point was arbitrarily taken as the integral time scale of turbulence. The arrows in figure 10 indicate the 'last' point for each correlation curve. One can, of course, use other physically meaningful and consistent definitions for the time scale. The present definition has been chosen because it was felt that the curve up to the first zero (i.e. the main lobe) represented the most significant part

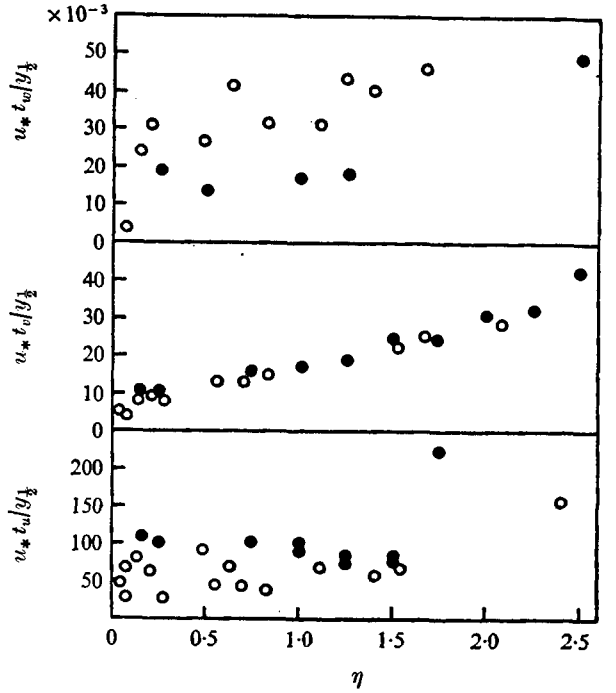

FIGURE 11. The distribution of the time scales t_u, t_v and t_w across the wall jet. ●, $x/t_c = 22$; ○, $x/t_c = 118$.

of the correlation curve, and its area would therefore give a very significant time scale. It was also possible to compute the time scale unambiguously in *all* the cases using this definition.

The integral time scales t_u, t_v and t_w for the two stations ($x/t_c = 22$ and 118) are plotted in figure 11. These time scales have been normalized, using a reference time scale $y_{\frac{1}{2}}/u_*$. It is seen that of the three scales only t_v shows Reynolds number independence. Further, while no significant trend in the variation of t_u and t_w can be observed, there is a systematic (nearly linear) variation in t_v. In fact, the trend is especially clear in the region which has the largest contribution to the total turbulent kinetic energy of the boundary-layer fluid.

Another significant observation that can be made from figure 11 is the difference among the magnitudes of the time scales (especially t_u and t_v). This can be seen more clearly from figure 12, where the ratio t_u/t_v is plotted for the two stations. It is seen that, at both stations, t_u/t_v has values of approximately 9–10 close to the wall, and drops to a value approaching 2 as the shear decreases to zero. This means that in strongly sheared flows the lifetime of v fluctuations is very much smaller than that of the u fluctuations. Use of Taylor's hypothesis for isotropic turbulence would lead us to expect t_u/t_v to be 2. The very large values of t_u/t_v in the strong shear regions can be qualitatively explained as follows

One can regard turbulence produced from mean shear to be initially contained in u fluctuations. This energy is later partly transferred to the other modes, v and w. This mechanism is fairly well accepted now. (See e.g. Rotta 1951.) It can

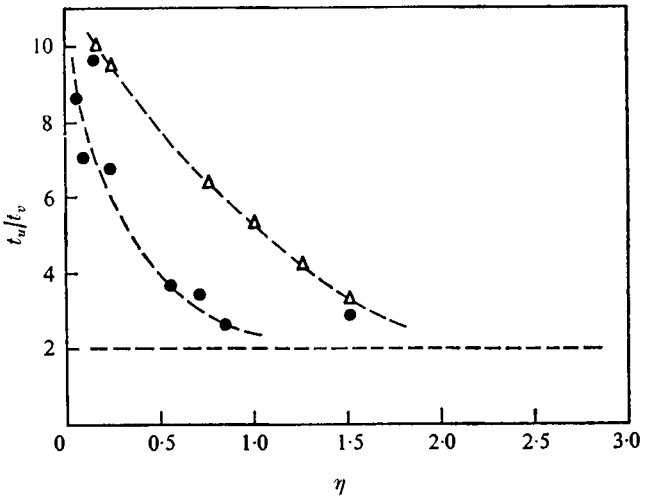

FIGURE 12. The distribution of t_u/t_v across the wall jet. ---△---, $x/t_c = 22$; ---○---, $x/t_c = 118$; ----, value of 2, for isotropic turbulence.

be expected to be prevalent, in the present case, at least at large distances from the slot. The Reynolds shear stress which represents the correlation between the u and v fluctuations is generated during the period of transfer of energy between these modes. It will now be hypothesized that the smaller time scale, viz. the time scale of the v fluctuations, corresponds to the duration of this transfer process. In other words, turbulent production occurs during these periods of duration t_v. The lifetime of the u fluctuations does not appear to vary significantly over the region of production, though it does depend upon the Reynolds number. The u–v transfer process becomes stronger and more frequent in regions of strong shear, resulting in larger values of t_u/t_v. As the outer limit of the production region is approached, the energy extracted from the mean shear decreases, and the transfer process becomes weaker and weaker. On the basis of this reasoning, one can expect t_v to be an important parameter characterizing turbulent production. The observation that t_v scales with u_* and $y_{\frac{1}{2}}$, the parameters with which all the other gross features of turbulence scale in the present case, points to t_v being a very relevant parameter, at least in the region of turbulent production.

The above argument leads to a possible model for the turbulent shear stress. The shear stress that represents the correlated portion of the u and v fluctuations will depend on the total turbulent kinetic energy, the strength of the u–v transfer process (which is dependent on $\partial\overline{U}/\partial y$) and the time scale of the transfer process (which has been seen to be t_v). Hence, one can write

$$\overline{uv} = \overline{uv}\{\overline{q^2}, t_v, \partial\overline{U}/\partial y\}. \tag{5.3}$$

Dimensional analysis yields

$$\overline{uv}/\overline{q^2} = F\{t_v\partial\overline{U}/\partial y\}. \tag{5.4}$$

Figure 13 shows a plot of $\overline{uv}/\overline{q^2}(t_v\partial\overline{U}/\partial y)$ for the two stations $x/t_c = 22$ and 118. While one must concede that the data show some scatter, it is still possible to

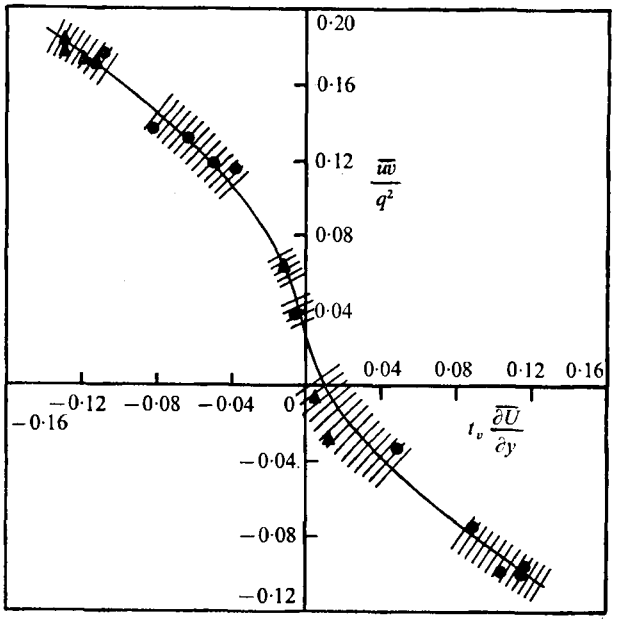

FIGURE 13. Dependence of Reynolds shear stress on $t_v \partial \overline{U}/\partial y$. ▲, $x/t_c = 22$; ●, $x/t_c = 118$. Hatching is done to bring out clearly the scatter in the measurements.

notice a definite trend as indicated by the hatched line. The positive values of $(t_v \partial \overline{U}/\partial y)$ obtained in the region very close to the wall may be somewhat in error, owing to the uncertainty in the measurements of both t_v and $\partial \overline{U}/\partial y$. But the figure indicates that the model implied by (5.4) is not unrealistic. A few other comments can also be made about this figure.

(i) Bradshaw's relation $\overline{uv} = a\overline{q^2}$ seems to be applicable to a flow only if $t_v \partial \overline{U}/\partial y$ is constant across the flow. The constant of proportionality depends on the state of the boundary layer as represented by $t_v \partial \overline{U}/\partial y$.

(ii) The anomaly around $\partial \overline{U}/\partial y = 0$ still persists as in the phenomenological models, because of the $\partial \overline{U}/\partial y$ term. But this is not a serious problem in practical calculations.

(iii) The quantity $t_v \partial \overline{U}/\partial y$ can be regarded as in some sense the ratio of the time scale of turbulence to that of mean shear. Generation of correlated turbulence relative to the total turbulence, as indicated by $\overline{uv}/\overline{q^2}$, thus appears to depend on this ratio.

(iv) It can be seen from the figure that the boundary-layer-like inner region of the wall jet behaves differently from the jet-like outer region, in that the values of $|\overline{uv}/\overline{q^2}|$ are smaller for the former for the same value of $|t_v \partial \overline{U}/\partial y|$. The reduced correlation between the u and v fluctuations in the inner layer of the wall jet is presumably due to the special features of the wall jet, viz. the production of the bulk of turbulent energy in the outer layer (see figure 15), and the existence of considerable interaction between the inner and outer layers. The present data for positive values of $\partial \overline{U}/\partial y$ are not, however, sufficiently exhaustive to reach a more definite conclusion. A more detailed study of this region, especially in thick wall jets, is probably worthwhile.

While the present limited data appear to support hypothesis (5.4), further experimental evidence from both wall jets and other shear flows is necessary to confirm its universality. It is for this reason that we refrain from giving a quantitative expression for F in (5.4) at this stage. But such an expression might eventually lead to a practically useful method for calculating wall-jet development. Of course, such a step presumes that one knows the distribution of t_v across the wall jet. One starting point would be to assume that the t_v distribution in figure 11 is also valid for wall jets subjected to arbitrary pressure gradients. Then figures 11 and 13 would together provide the closure for the momentum equation. The extension of the scheme to other shear flows, however, depends to a great extent on the confirmation of the universality of (5.4) and the information available on the t_v distribution. Further work in this direction is in progress.

6. Turbulent energy spectra

6.1. *Spectrum measurements*

As already stated, frequency spectra of u'^2, v'^2 and w'^2 were obtained directly from the digitized data of u, v and w, using the technique of fast Fourier transforms. 2048 samples were used for the transform, out of the 3000 samples available in each batch. Stability was improved by hanning. Each spectrum was obtained as the average over 30 batches, spread over 30 s. The effective window width B_e was about 13 Hz. The value of e for this case can be calculated from

$$e \approx (B_e T_s)^{-\frac{1}{2}} \approx 0{\cdot}05.$$

(See Magrab & Blomquist 1971.) The equivalent number of degrees of freedom, for an assumed chi-square distribution for the power spectral function, is $2B_eT_s = 780$. This corresponds roughly to confidence limits of $\pm 0{\cdot}35$ db (i.e. approximately $\pm 8{\cdot}5$ %) in the spectral function, based on a 90 % expectation.

The spectra were obtained at several points across the wall jet, at the two longitudinal stations $x/t_c = 22$ and 118. Define the wavenumber k_1 as

$$k_1 = 2\pi f/\overline{U}.$$

(f is the frequency.) Then one can compute the one-dimensional spectrum functions in wavenumber space from the frequency spectra. It is assumed here that Taylor's relation is valid, in the form $\partial/\partial t = \overline{U}\,\partial/\partial x$. Again, while more than 40 wavenumber spectra were computed, only a typical set is presented in figure 14. In this figure, the spectrum function and wavenumber are normalized using $\overline{q^2}$ and $y_{\frac{1}{2}}^{-1}$, respectively. The non-dimensional spectrum function $\phi(y_{\frac{1}{2}}k_1)$ is defined in the usual way, so that

$$\int_0^\infty \phi_{u^2}(y_{\frac{1}{2}}k_1)\,d(y_{\frac{1}{2}}k_1) = \overline{u^2}/\overline{q^2}, \tag{6.1}$$

and so on for v'^2, w'^2 and $\overline{q^2}$.

Since the low-pass analog filter lowered the frequency response beyond 6 kHz, the spectral calculations could not, in many cases, be extended with accuracy far enough into the Kolmogorov range. But this does not affect the conclusions to be drawn from the spectra up to a frequency of 6 kHz. In fact, the spectra shown

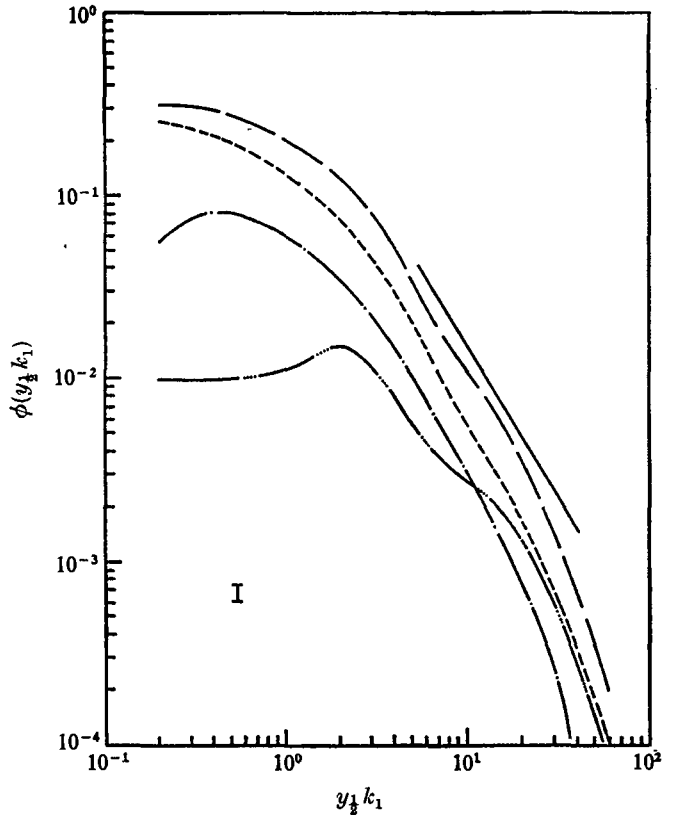

FIGURE 14. One-dimensional energy spectra at $x/t_c = 118$ and $y = 1{\cdot}4$ in. – – – –, $\phi_{u^2}(y_{\frac{1}{2}}k_1)$; —·····—, $\phi_{v^2}(y_{\frac{1}{2}}k_1)$; —·—·—, $\phi_{w^2}(y_{\frac{1}{2}}k_1)$; ————, $\phi_{q^2}(y_{\frac{1}{2}}k_1)$; ——, line of slope $-\frac{5}{3}$. The height of the vertical bar indicates the extent of uncertainty in the results.

in figure 14 extend up to only 5 kHz. It was observed, that, with a few exceptions, the computed spectra generally indicated near-isotropy towards the high-wavenumber end. The deviation in a few cases from this general trend (such as e.g. the w'^2 spectrum in figure 14) is presumably due to errors in measurement at the high-wavenumber end. But no definite explanation can be given for this. We shall, therefore, simply state that there appears to be a general tendency towards isotropy at the high-frequency end of the measured spectrum.

Since, in the present case, turbulent energy production takes place over a substantial region away from the wall (up to $\eta = 1{\cdot}5$), it has been possible to obtain v'^2 and w'^2 spectra at a number of points in the region of production. This is normally difficult, if not impossible, in a conventional boundary layer. It is seen from figure 14 that the v'^2 and w'^2 spectra exhibit a local maximum. This feature was observed in all the spectra. The maximum in the v'^2 spectrum was observed at a non-dimensional wavenumber $y_{\frac{1}{2}}k_1 = k_1^* \approx 2$, in all cases. The existence of such a peak was not clearly observable in the u'^2 spectra while the wavenumber k_1^*, at which the peak occurred in the w'^2 spectra, varied from 0·5 to 2·0. The existence of these peaks is also suggested by the autocorrelation curves in figure 10, and it indicates some kind of periodicity in the flow. It is possible that

this periodicity is due to the slot-tip vortices convected downstream by the flow. But it is interesting that the non-dimensional 'eddy size' $L/y_{\frac{1}{2}}$, corresponding to the peak in the spectra, works out to be between 3 and 6 in most cases. (L is defined as $2\pi y_{\frac{1}{2}}/k_1^*$.) This agrees approximately with the non-dimensional distance between high-frequency turbulent 'bursts' observed by Rao, Narasimha & Badri Narayanan (1971) in a boundary layer. This fact suggests the alternative possibility that the humps in the spectra may indicate the high frequency turbulent 'bursts' now believed to be a characteristic feature of turbulence production. (See also e.g. Kline *et al.* 1967.) Detailed study of the periodicity was not made in the present investigation, however.

6.2. *Dissipation rate from spectrum*

Lawn (1971) reported that a kind of isotropy, described by Bradshaw as 'second class', is observable in pipe flows at Reynolds numbers considerably smaller than that required for obtaining a distinct equilibrium range in the spectrum. In this range of second-class isotropy, the shear-stress spectrum $E_{uv}(k_1)$, while falling off rapidly, will have still an appreciable value while the energy spectra $E_{u^2}(k_1)$ and $E_{v^2}(k_1)$ exhibit near-isotropy. Even prior to this, the u'^2 and v'^2 spectra start showing a $k_1^{-\frac{5}{3}}$ variation. Bradshaw found that, under this condition,

$$E_{u^2}(k_1) = K\epsilon^{\frac{2}{3}}(k_1)^{-\frac{5}{3}} \tag{6.2}$$

is satisfied, where ϵ is the dissipation rate and the non-dimensional spectrum functions $E(k_1)$ are defined by the usual relations of the type

$$\int_0^\infty E_{u^2}(k_1)\,dk_1 = u'^2,$$

etc. The value of K has been found to be 0·5–0·55 in a boundary layer. Lawn showed that this condition can be obtained in pipe flow, if the Reynolds number of turbulence $Re_\lambda = u'\lambda_{xu}/\nu \geqslant 140$. ($\lambda_{xu}$ is the micro-length scale of the u fluctuations in the x direction.) His work indicated that (6.2)could conveniently be used for calculating the dissipation rate from spectrum measurements at frequencies lower than the dissipative range frequencies.

It was felt that it would be worthwhile to examine the present data in the light of the above. A line of slope $-\frac{5}{3}$ is drawn in figure 14. It is seen from the figure that, in the region where the u'^2 spectrum appears to have a $-\frac{5}{3}$ slope, there is no indication of the isotropy relation being satisfied among the three spectra. This was observed in most cases. Nevertheless, taking advantage of the fact that the $-\frac{5}{3}$ power variation would be exhibited even *prior* to the occurrence of 'second-class isotropy', one can still seek to compute the rate of dissipation from this region of the spectrum. However, in view of the lack of isotropy, it was decided to use the $\overline{q^2}$ spectrum for this purpose, instead of the u'^2 spectrum. It can be seen from figure 14 that the $\overline{q^2}$ spectrum does indicate a $-\frac{5}{3}$ power variation over a range of wavenumbers. This feature was observed in all cases. All the measured $\overline{q^2}$ spectra exhibited a $-\frac{5}{3}$ power variation over a part of the region

$$5 < (y_{\frac{1}{2}}k_1) < 20,$$

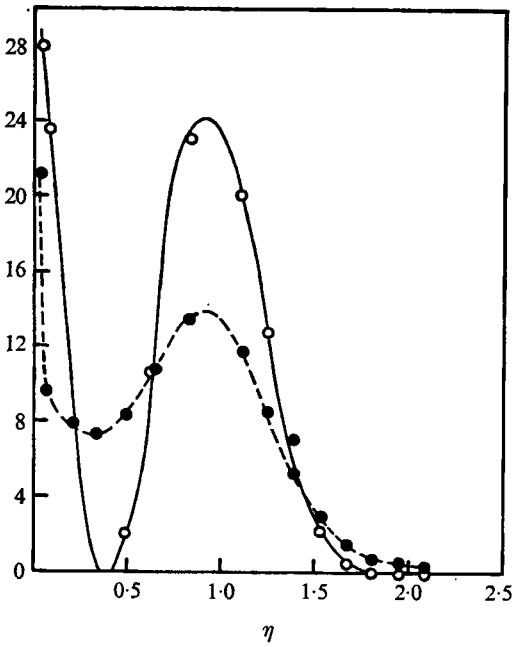

FIGURE 15. Production and dissipation of turbulent kinetic energy across the wall jet. —○—, $(-\overline{uv}/u_*^3)(\partial\overline{U}/\partial y)y_{\frac{1}{2}}$; —●—, $\epsilon y_{\frac{1}{2}}/u_*^3$ from (6.3).

though the exact extent of the wavenumber range over which this trend existed was slightly different for different spectra. It was decided to exploit this feature to compute dissipation in the wall jet, using a slightly modified version of (6.2).

From an analysis of Lawn's data on pipes, one can rewrite (6.2) as

$$E_{q^2}(k_1) = C_1 k_1^{-\frac{5}{3}} \epsilon^{\frac{2}{3}}. \tag{6.3}$$

(C_1 is a universal constant.) The value of C_1, from Lawn's data, works out to be 1·45. Figure 15 shows the dissipation rate calculated using (6.3) for the station $x/t_c = 118$. Unfortunately, results from other methods of estimation are not available for checking the accuracy of the present one. Also, detailed measurements were not made in the present investigation to gather information on the turbulent energy balance. But an approximate integral energy balance check can be made. Figure 15 also shows the distribution of the rate of turbulent energy production. From the figure, the rate of production of total turbulent energy at the section exceeds that of dissipation by nearly 20 %. Since the net lateral rate of diffusion must be zero, this excess must be convected downstream. However, calculation of the net rate of convection from the section indicated that it accounted for a negligible part of this difference. This discrepancy indicates that perhaps the dissipation values obtained from (6.3) are low by about 20 %. But, it is possible, too, that the discrepancy is partly due to any non-axisymmetry present in the flow.

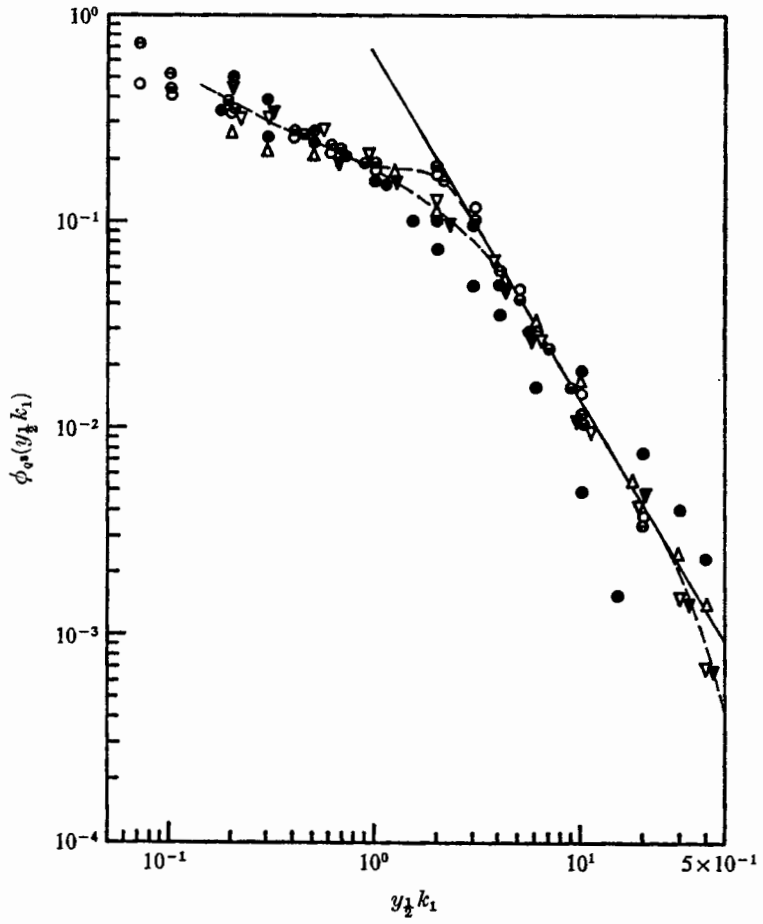

FIGURE 16. Non-dimensional spectra of $\overline{q^2}$, exhibiting near-similarity. ——, distribution $\phi_{q^2} = 0{\cdot}64\ (y_{\frac{1}{2}}k_1)^{-\frac{5}{3}}$; – – –, mean through the data points. Note the hump in the region of $y_{\frac{1}{2}}k_1 = 2$.

	○	◒	⊖	⊕	●	△	▽	▼
x/t_c	22	22	22	22	118	118	118	118
y (in.)	0·1	0·3	0·5	1·0	0·1	0·4	1·4	2·4
				($\eta = 2{\cdot}5$)	($\eta = 0{\cdot}07$)			

6.3. *Self-similarity of the $\overline{q^2}$ spectrum*

In figure 16, the non-dimensional spectra of $\overline{q^2}$ for the different points in the wall jet at the two longitudinal stations $x/t_c = 22$ and 118 are plotted again. It is seen that the spectra collapse on one another in the region $5 < (y_{\frac{1}{2}}k_1) < 20$, except for the two extreme values of $\eta = 2{\cdot}5$ at $x/t_c = 22$, and $\eta = 0{\cdot}07$ at $x/t_c = 118$. It thus appears that, in the above wavenumber range (except in the neighbourhood of the hump around $y_{\frac{1}{2}}k_1 = 2$), the spectrum exhibits a self-similar distribution of the form

$$\phi_{q^2} = C(y_{\frac{1}{2}}k_1)^{-\frac{5}{3}}. \tag{6.4}$$

(C is a constant.) In fact, as indicated by the dashed line in figure 16, the similarity in $\overline{q^2}$ spectra extends approximately even to as low a non-dimensional wavenumber as 0·2. Hence, spectra over most of the boundary layer scale with a single length scale, viz. the characteristic length scale $y_{\frac{1}{2}}$ (except probably very close to the wall). But this is true for only the $\overline{q^2}$ spectrum, not for the u'^2, v'^2 or w'^2 spectra. In the latter, self-similarity is not observed, unless one goes to the region of at least second-class isotropy. This is due to the preferential extraction of energy by the u component, and transfer to the v and w modes in the lower wavenumber regime.

Now, for the region of $-\frac{5}{3}$ slope, one can write

$$E_{q^2}(y_{\frac{1}{2}} k_1) = \overline{q^2} C (y_{\frac{1}{2}} k_1)^{-\frac{5}{3}}. \tag{6.5}$$

Using

$$E_{q^2}(k_1) = y_{\frac{1}{2}} E_{q^2}(y_{\frac{1}{2}} k_1), \tag{6.6}$$

and combining (6.5) with (6.3), one gets

$$\epsilon y_{\frac{1}{2}}/u_*^3 = (C/C_1)^{\frac{3}{2}} (\overline{q^2}/\overline{u_*^2})^{\frac{3}{2}}. \tag{6.7}$$

The constant C is not universal, and obviously depends on the scaling length chosen. For the present case, where $y_{\frac{1}{2}}$ is chosen as the length scale, C works out to be 0·64.

Substituting the numerical values of C and C_1 in (6.7), one gets

$$\epsilon y_{\frac{1}{2}}/u_*^3 = 0{\cdot}292 (\overline{q^2}/u_*^2)^{\frac{3}{2}}. \tag{6.8}$$

The expression (6.8) is of familiar form, with the qualification that the length scale can be taken as $y_{\frac{1}{2}}$ almost right across the wall jet. Since the $\overline{q^2}$ distribution exhibits near self-similarity, it follows from (6.8) that the dissipation rate also would exhibit a similar behaviour. This self-similar distribution is given by that shown in figure 15 for the station $x/t_c = 118$.

7. Conclusion

The investigation has led to the following conclusions

(i) Axisymmetric wall jets under adverse pressure gradients exhibit a self-similar structure in the outer layer, provided the pressure-gradient parameter β is small. The self-similarity is observed first in the mean velocity profile. But, it appears to extend to the distribution of many turbulent quantities, at a sufficiently large distance from the slot.

(ii) The distribution of the shear stress over the outer region of the wall jet can be described satisfactorily by simple, available, turbulence hypotheses. These hypotheses fail to describe the wall region satisfactorily, however.

(iii) The time scales of the u and v components of turbulent velocity fluctuations show a very great difference between their magnitudes in regions of high shear. The time scale of v fluctuations appears to be the most relevant of the three time scales for determining the magnitude of the Reynolds stress.

(iv) The ratio $-\overline{uv}/\overline{q^2}$ appears to be a strong function of the ratio of the time scale of v fluctuations to a typical time scale of mean shear, viz. $(\partial \overline{U}/\partial y)^{-1}$.

(v) The rate of dissipation computed from the spectra of $\overline{q^2}$ from (6.3) [or (6.8)], which is a modified version of Bradshaw's recommendation, appears to be qualitatively reasonable, though it is probably too low by about 20 %.

(vi) One-dimensional spectra of $\overline{q^2}$ exhibit a $-\frac{5}{3}$ power law variation over a range of wavenumbers, lower than that at which the u'^2, v'^2 and w'^2 spectra tend towards isotropy. In this range, a self-similar behaviour is observable in the $\overline{q^2}$ spectra in the region of turbulence production (except very close to the wall), if the local mean velocity $\bar{U}$ and half-width $y_{\frac{1}{2}}$ are used for forming the non-dimensional wavenumber. In fact, the self-similarity in $\overline{q^2}$ spectra extends approximately down to $y_{\frac{1}{2}} k_1 = 0{\cdot}2$.

The author gratefully acknowledges financial support received from the Defense Research Board of Canada and the University of Waterloo, Waterloo, Ontario, Canada, while the experimental data were obtained. He also wishes to thank Professor W. B. Nicoll of the University of Waterloo, for many useful discussions.

REFERENCES

BLACKMAN, R. B. & TUKEY, J. B. 1958 *Measurement of Power Spectra from the Point of View of Communication Engineering.* Dover.

BRADSHAW, P., FERRISS, D. H. & ATWELL, N. P. 1967 Calculation of boundary-layer development using the turbulent energy equation. *J. Fluid Mech.* **28**, 593.

KACKER, S. C. & WHITELAW, J. H. 1968 Some properties of the two-dimensional turbulent wall jet in a moving stream. *Trans. A.S.M.E., J. Appl. Mech.* E **35** (4), 641–651.

KLINE, S. J., REYNOLDS, W. C., SCHRAUB, F. A. & RUNSTADLER, P. W. 1967 The structure of turbulent boundary layers. *J. Fluid Mech.* **30**, 741–773.

KOLMOGOROV, A. N. 1942 *Izv. Akad. Nauk SSSR, Ser. Phys.* **1**, 2.

KRUKA, V. & ESKINAZI, S. 1964 The wall jet in a moving stream. *J. Fluid Mech.* **20**, 555–579.

LAWN, C. J. 1971 The determination of the rate of dissipation in turbulent pipe flow. *J. Fluid Mech.* **48**, 477–505.

MAGRAB, E. B. & BLOMQUIST, D. S. 1971 *The Measurement of Time-Varying Phenomena.* Interscience.

NEWMAN, B. G., PATEL, R. P., SAVAGE, S. B. & TJIO, H. K. 1972 Three-dimensional wall jet originating from a circular orifice. *Aero. Quart.* **22**, 188–200.

NICOLL, W. B. & RAMAPRIAN, B. R. 1970 Performance of conical diffusers with annular injection at inlet. *Trans. A.S.M.E., J. Basic Engng,* D **92**, 827–835.

RAMAPRIAN, B. R. 1969 Conical diffusers with annular injection at inlet. Ph.D. thesis, Department of Mechanical Engineering, University of Waterloo, Canada.

RAMAPRIAN, B. R. 1973 Turbulent wall jets in conical diffusers. *A.I.A.A. J.* **11**, 1684–1690.

RAO, K. N., NARASIMHA, R. & BADRI NARAYANAN, M. A. 1971 The 'bursting' phenomena in a turbulent boundary layer. *J. Fluid Mech.* **48**, 339–352.

ROTTA, J. 1951 Statistiche Theorie nichthomogener Turbulenz. *Z. Phys.* **129**, 547–572. (Trans. W. Rodi 1968 *Dept. Mech. Engng, Imperial College, Rep.* TWF-TN-38.)